Gas puff modulation experiments in JET L- and H-mode plasmas

A. Salmi[1], T. Tala[1], C. Bourdelle[2], P. Mantica[3], L. Meneses[4], S. Mordijck[5], H. Bufferand[2], M. Clever[6], J. Svensson[7], P. Tamain[2], M. Groth[8], J. Hillesheim[9], C. Maggi[10], M. Maslov[9], V. Naulin[11], J. Juul Rasmussen[11], G. Sips[12], A. Sirinelli[13], M. Tsalas[14], H. Weisen[15], M. Wischmeier[10] and JET-EFDA contributors*
JET-EFDA, Culham Science Centre, Abingdon, OX14 3DB, UK
[1]VTT, Espoo, Finland; [2]IRFM-CEA, Saint Paul lez Durance, France; [3]IFP, CNR-ENEA, Milan, Italy; [4]IST, Lisbon, Portugal; [5]College of William & Mary, Virginia, USA; [6]FZJ, Jülich, Germany, [7]IPP, Greifswald, Germany, [8]Aalto University, Helsinki, Finland; [9]CCFE, Abingdon, UK; [10]IPP, Garching, Germany; [11]DTU Physics, Lyngby, Denmark; [12]EFDA CSU, Culham, [13]ITER, France, [14]DIFFER, Nieuwegein, Netherlands; [15]CRPP, Lausanne, Switzerland.

JET experiments utilising gas puff modulation technique [1-5] have been carried out in both L- and H-mode plasmas to study plasma fuelling through the pedestal as well as particle sources and transport. The H-mode experiment is the first exploration of this technique on JET H-mode conditions and focuses on verifying the potential of this technique. The modulation technique, equations and the H-mode experiment (ITER like wall) are described first while the L-mode collisionality scan results (Carbon wall) are given at the end.

Experimental setup

The H-mode discharges are run in the corner configuration with low triangularity, B_t=2.7T, Ip=2.0MA, n_{e0}=6x10^{19}m^{-3}, T_{e0}=3.5keV. Figure 1 illustrates the various gas injection locations used in these discharges on poloidal plane. The top and midplane GIMs can be considered as point sources while the ones at the divertor are nearly axisymmetric. GIM 12 was on in all discharges with constant gas rate of ~1.5e22 1/s while the others were modulated (one at a time) using 2-4 Hz rectangular waveform with 50% duty cycle going from 0 to ~1.5e22 1/s. The small equilibrium modulation due to the gas is removed by mapping the data on flux coordinates before calculating the amplitude and phase profiles. The plasma response (electron density modulation) is measured with a multi-band reflectometer (KG10) capable of good spatial and temporal resolution [6]. This data was found to agree well with the Thomson Scattering both in steady state and in temporal response.

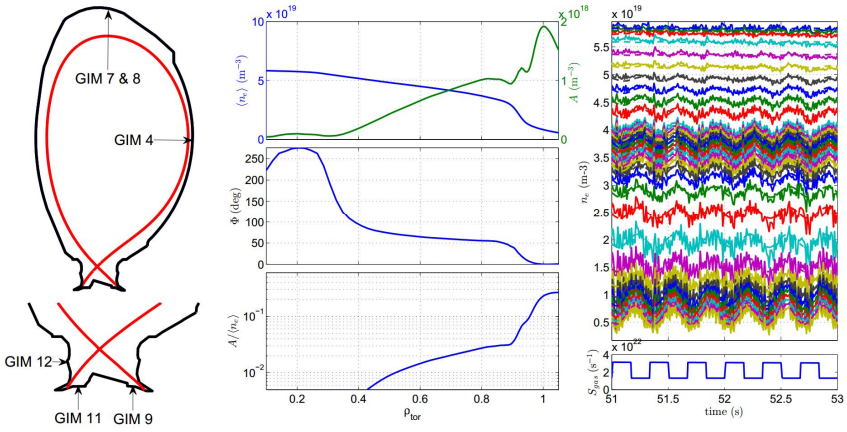

Figure 1 (left) Approximate gas injection locations in poloidal plane (middle) electron density profile and the modulation amplitude and phase profiles at 3 Hz for #85231 (right) gas modulation waveform and the temporal density traces from reflectometer.

Electron density evolution

In interpreting the measurements we assume that the electron density evolution follows the usual 1.5D equation for non-cylindrical and axisymmetric plasmas and that the transport does not evolve in time

$$\frac{\partial}{\partial t}(V' n_e) = \frac{\partial}{\partial \rho}\left[V'\langle(\nabla\rho)^2\rangle\left(D\frac{\partial n_e}{\partial \rho} - v n_e\right)\right] + V'S. \quad (1)$$

Here ρ is the normalised square root of toroidal flux, $V'(\rho)$ is the radial derivate of the plasma volume, $D(\rho)$ and $v(\rho)$ are the diffusion and convection profiles, $S(\rho,t)$ is the particle source and $\langle\ \rangle$ denotes flux surface averaging.

We utilise this equation in two ways to solve the underlying transport. In one case the Eq. (1) is solved inside a loop where non-linear optimisation algorithm is adjusting the transport coefficients D and v until best fit in χ^2 sense is found simultaneously for the modulated amplitude, phase and the steady state profiles. Time independent flux boundary condition is used at the outer boundary. Due to the uncertainty of the cold neutral source its magnitude (both the steady state and modulated part) are also fitted for best match while the shape of the profile is given by FRANTIC. The second way of using Eq. (1) is explained the next section.

D and v from the measured amplitude and phase profiles

For any periodic perturbation with time independent transport one can use the measured amplitude and phase profiles of the perturbation to calculate the transport coefficients D and v [8]. In Ref. [8] these formulas were derived in a cylindrical plasma approximation. For completeness we write D and v starting from the more general geometry included in Eq. (1) while also retaining the source term. Using the same notation and the ansatz $n(\rho,t) = n_0(\rho) + A(\rho)\sin(\omega t - \varphi(\rho))$ together with $S(\rho,t) = S_0(\rho) + A_s(\rho)\sin(\omega t - \varphi_s(\rho))$ we arrive at similar equations:

$$D = -\omega\frac{Y\sin\varphi + X\cos\varphi}{A\varphi' V'\langle(\nabla\rho)^2\rangle}, \quad v = -\omega\frac{(A'Y - \varphi' AX)\sin\varphi + (\varphi' AY + A'X)\cos\varphi}{A^2\varphi' V'\langle(\nabla\rho)^2\rangle} \tag{2}$$

$$X = \int V'\left(A\cos\varphi + \frac{A_S}{\omega}\sin\varphi_S\right)d\rho, \quad Y = \int V'\left(A\sin\varphi - \frac{A_S}{\omega}\cos\varphi_S\right)d\rho$$

Figure 2 summarises the D and v profiles for the H-mode data set (#85228 - #85232) where GIM 4 was used using Equations (2) while neglecting any modulated source terms (valid inside 0.8). It is seen that in cases where the same modulation frequency was used the same amplitude profile is obtained with good accuracy. Another clear observation is that the measured amplitude increases with decreasing frequency as expected. Furthermore, the derived convective velocity is outwards (bottom frame). This is not compatible with the peaked steady state profile that in fact requires inward convection given the relatively small central fuelling from NBI.

It is possible to achieve a relatively good fit which simultaneously reproduces the observed steady state electron density but this requires sacrificing the perfect match in amplitude and phase. This is shown in Figure 3 where the iterative approach for solving D and v profiles is used. Clearly, the rapidly decaying amplitude and the flat phase are not matched exactly without outward convection. The same conclusion was obtained also in ASTRA transport code simulations. Some potential explanations for this are given below.

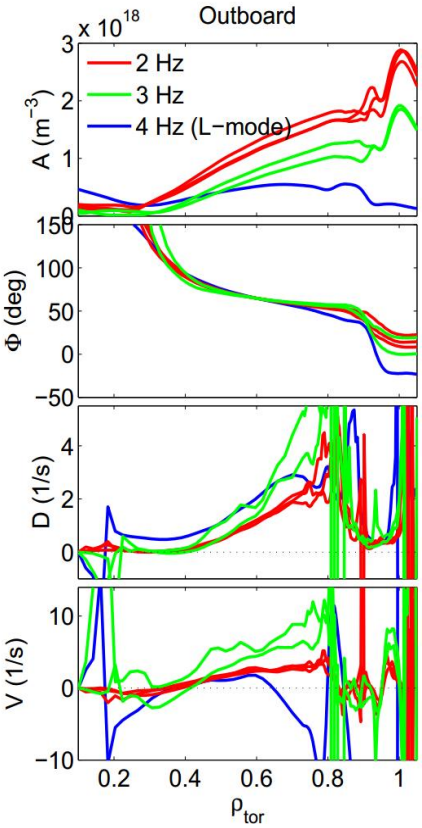

Figure 2 (top rows) Amplitude and phase profiles and (bottom rows) the D and V profiles of the GIM 4 data set.

ELMs and sawteeth

These discharges have both sawteeth (~4 Hz) and ELMs (~50 Hz) on top of the gas modulation induced transients. The effect of the gas puff modulation is completely masked by the sawteeth when their frequencies match too closely. In practise all of the 4 Hz gas modulation phases in H-mode were found unusable. During an ELM particle transport increases significantly and cannot be considered to be time independent like we assume when solving transport from Eq. (1). However, since within each modulation cycle several ELMs occur the transport we are solving is ELM-averaged transport which is time independent by definition. The remaining caveat is that ELM frequency itself is somewhat modulated by the gas puff modulation. Present analysis neglects this effect which could potentially change the transport at the gas modulation frequency.

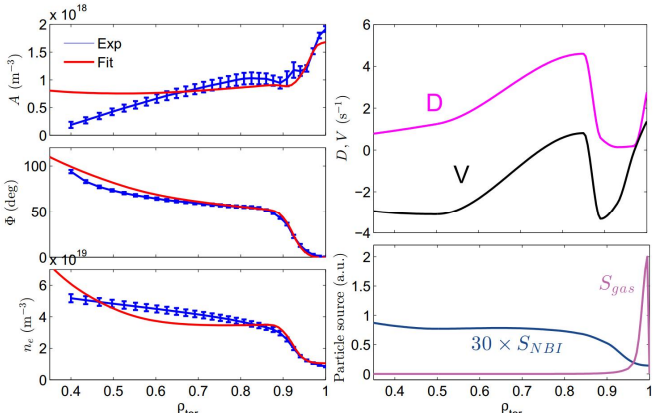

Figure 3 (left) Experimental and best fitting amplitude, phase and steady state for #85231 with GIM 4 modulation (right) the transport and source profiles.

The complex particle source

The difficulties in simultaneously fitting the steady state and the perturbed amplitude and phase profiles may also be originating from too simplistic cold neutral source terms used in the modelling. Figure 5 shows tomographic inversion [9] of KL11 [10] data (Dα video at 60 Hz) on poloidal plane for #85231 which feature both GIM 4 and GIM 8 modulation phases. Inversion has been done in the Minerva framework [11]. Note that the divertor GIM 12 was constantly on. In frame *b* the modulated emission reveals three distinct regions in the divertor area that contribute to the total modulated source: *1)* direct source aligned with LFS separatrix, *2)* recycling source on the inner divertor apron and *3)* a volume source just left from the X-point. Of course one must keep in mind that the data is Dα light and that proper interpretation requires SOL modelling. One can also see that modulations occur at different delays (frame *d*): The LFS radiation comes first and the HFS emission lags some 40 ms behind. Interestingly the volume emission is in anti-phase with the LFS emission. The frames

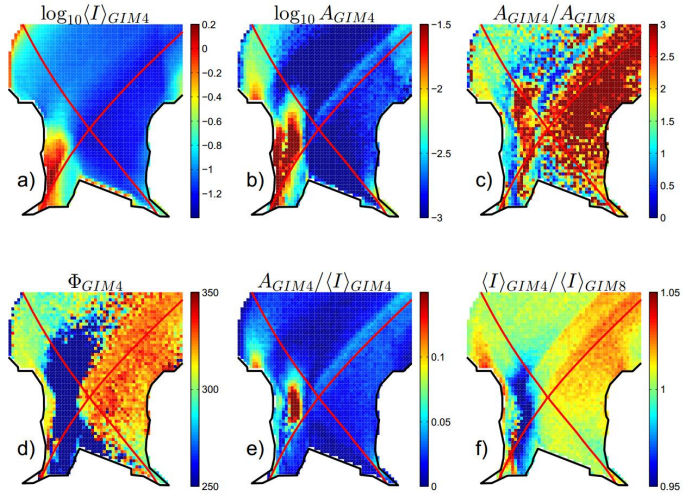

Figure 5 Dα image data tomographically inverted [9] onto poloidal plane. a) time averaged intensity on log scale, b) 3 Hz modulation amplitude on log scale, c) 3 Hz amplitude ratio between GIMs 4 and 8, d) 3 Hz modulation phase, e) ratio between the 3 Hz modulation and steady state Dα intensity, and f) Dα ratio between GIMs 4 and 8.

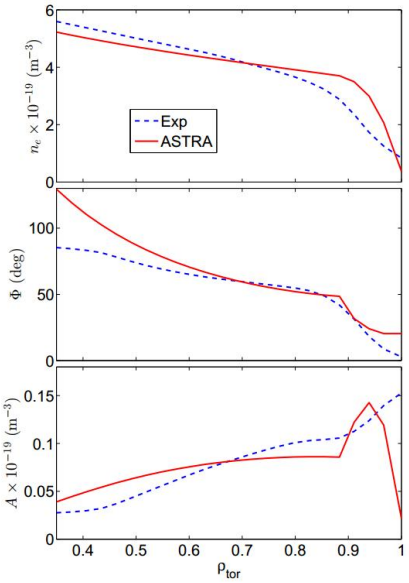

Figure 4 ASTRA fit with warm neutral contribution.

c and *f* show the differences between GIM 4 and 8 confirming the expected trends. These data have not yet been fully utilised in SOL modelling but will provide valuable information for future work trying to clarify the particle sources. Further evidence for the need of better source understanding is shown in Figure 4 where an improved match was obtained in an exploratory ASTRA simulation that used warm neutrals (250 eV) in addition to the 2 eV cold neutrals.

L-mode collisionality scan

The gas modulation technique described above was also utilised in JET L-mode plasmas. These, yet unreported, discharges form a dimensionless 3-point collisionality scan which was achieved by changing temperature through NBI while keeping the density constant. As seen in Figure 6, the calculated profiles are roughly equal inside 0.6 where the modulated particle source is expected to be very small. This is consistent with the earlier experimental database study on JET [7] where in L-mode no collisionality dependence in density peaking was found. The result was also confirmed by a gyrokinetic quasi-linear analysis using QuaLiKiz [14] that found no trends within the scan However, it is noted that weak collisionality dependence in the relevant L-mode parameter range was found with QuaLiKiz when using artificial parameters nulling the small but unavoidable Te/Ti changes in the experimental scan.

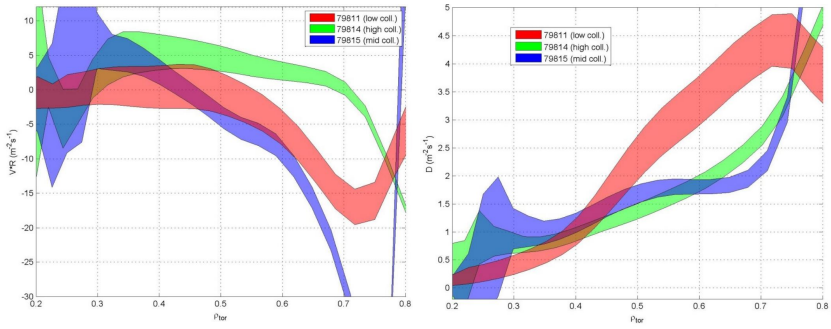

Figure 6 Derived D and V profiles for the L-mode collisionality scan. Note that the error estimate only takes into account the fluctuations in amplitude and phase profiles that depend on the choice of the time window.

Discussion and conclusion

JET L-mode gas modulation experiments have shown that collisionality is not strongly affecting the particle transport, consistent with earlier experiments. The H-mode discharges in JET utilising this technique have shown that perturbation due to the modulated gas puff is reproducible with good accuracy thereby suggesting that the scheme has potential for future JET studies of H-mode particle transport e.g. by scanning q and collisionality. It was seen that gas modulation frequency must not coincide with sawtooth frequency in order to obtain reliable data. The measured electron density and the propagation of the density wave due to the gas puff have so far not been exhaustively explained. Several possibilities for resolution exist and include at least the NBI particle source modulation due to the density modulation, transport modification due to ELM frequency modulation and the additional complexities of the cold neutral source suggested by the Dα camera data (see Figure 5). The inclusion of these factors is left for future work.

This work was supported by EURATOM and carried out within the framework of the European Fusion Development Agreement. The views and opinions expressed herein do not necessarily reflect those of the European Commission.

References

[1] K.W. Gentle et al 1992 NF 32 217
[2] J O'Rourke et al 1993 PPCF 35 585
[3] K. Nagashima et al 1993 NF 33 1677
[4] D.R. Baker et al 1998 NF 38 485
[5] E. Doyle et al 2012 Proc. IAEA FEC
[6] A. Sirinelli et al 2010 RSI 81 10D939
[7] H. Weisen et al 2005 NF 45
[8] H Takenaga et al 1998 PPCF 40 183
[9] J. Svensson 2011 EFDA–JET–PR(11)24
[10] A. Huber et al 2012 RSI 83
[11] J. Svensson et al 2007 Proc. IEEE WISP
[12] R. Pasqualotto et al 2004 RSI 75
[13] C.D. Challis et al 1989 NF 29 563
[14] C. Bourdelle et al 2007 PoP 14, 112501
* *F. Romanelli et al, Fusion Energy 2012 (Proc. 24th IAEA Conf., San Diego, 2012) IAEA Vienna*